PHOTONICS Research

Zeolite templated carbon nanodots for broadband ultrafast pulsed fiber laser generation

Xintong Xu,[1,2] Jiaqi Chen,[2] Wentao Shi,[2] Dalin Sun,[2] Shaowen Chu,[2] Lang Sun,[2] Wenfei Zhang,[2] Yanping Chen,[3] Jianpang Zhai,[3] Shuangchen Ruan,[1,2,*] and Zikang Tang[4]

[1]Center for Advanced Material Diagnostic Technology, College of Engineering Physics, Shenzhen Technology University, Shenzhen 518118, China
[2]Shenzhen Key Laboratory of Laser Engineering, Shenzhen University, Shenzhen 518060, China
[3]College of New Materials and New Energies, Shenzhen Technology University, Shenzhen 518118, China
[4]Institute of Applied Physics & Materials Engineering, Faculty of Science and Technology, University of Macau, Macau, China
*Corresponding author: scruan@sztu.edu.cn

Received 29 April 2019; revised 27 July 2019; accepted 14 August 2019; posted 15 August 2019 (Doc. ID 366262); published 1 October 2019

Carbon nanodots (C-dots) with a uniform size of about 2 nm are synthesized via *in situ* pyrolysis of n-propylamine that is confined in the nanochannels of zeolite Linde Type A (LTA). The as-synthesized C-dots@LTA composite shows nonlinear optical saturable absorption properties in a broad wavelength band and can be used as saturable absorber (SA) to generate ultrafast pulsed fiber lasers. By inserting a zeolite LTA single crystal hosting C-dots into the fiber laser cavity, mode-locked fiber lasers with long-term operation stability at 1.5 μm and 1 μm are achieved. These results show that the C-dots@LTA are a promising SA material for ultrafast pulsed fiber laser generation in a broad wavelength band. To the best of our knowledge, this is the first demonstration of a C-dots@LTA-based mode-locked fiber laser.

https://doi.org/10.1364/PRJ.7.001182

1. INTRODUCTION

Since its discovery in 2004, carbon nanodots (C-dots) have gained much attention due to their fantastic advantages of low toxicity, biocompatibility, water solubility, and excellent photostability [1–5]. Owing to the excellent fluorescence properties of C-dots in an aqueous solution, various applications based on C-dots have been investigated, such as bioimaging probe [6,7], metal ion detection [8], and photocatalysis [9,10]. However, the performance of optical devices based on C-dots is highly limited for its aggregation-induced quenching effects when they are dried into films or powders. Recently, a template-supported strategy has been used to investigate the optical property of C-dots in solid state through embedding C-dots into tremendous host matrices [11,12]. Among them, zeolite has emerged as an ideal template to synthesize C-dots for its various identical nanopore systems and high thermal stability [13–16]. The solid state C-dots@zeolite shows specific optical properties, such as multicenter photoluminescence [17], long lifetime, and phosphorescence [18,19]. Despite the large advance in C-dot synthesis and application, the nonlinear optical saturable absorption properties and its application in ultrafast pulsed laser generation are seldom explored [20]. It is noted that ultrafast pulsed lasers with mode-locking have wide applications in optical telecommunication, biomedical diagnostics, and laser precision manufacturing [21–23].

A nonlinear optical element called a saturable absorber (SA) was widely used to generate ultrafast pulsed fiber lasers. In the past decades, a semiconducting saturable absorber mirror (SESAM) has been developed as a promising SA to generate ultrafast fiber lasers [24]. However, the SESAM's fabrication process is complicated and expensive, greatly limiting its further application. Recently, low-dimensional materials, such as carbon nanotubes [25–28], graphene [29–32], graphene oxide [33–35], topological insulators [36–40], black phosphorus [41], and layered metal dichalcogenides have been investigated as SAs to generate ultrafast pulsed fiber lasers [42–44]. However, there are a few drawbacks associated with these materials for ultrafast photonics devices. For example, many of these SA materials are composited with polymer, which have a drawback of poor dispersity and are inclined to aggregation, inducing the instability of photonics devices. Besides, these SA materials can operate at only a relatively low pump power for the unavoidable thermal effect on the polymer at a high incident laser power. It is therefore of great importance to find new nonlinear materials with low cost, good stability, and a high optical damage threshold in broadband laser operation.

In this work, we present the fabrication of C-dots with a uniform size by pyrolysis of an n-propylamine (NPA) that is confined in zeolite Linde Type A (LTA) topology. The C-dots@LTA exhibits nonlinear saturable absorption properties at 1.5 μm and 1 μm. By inserting the C-dots@LTA SA into the fiber laser cavity, mode-locked ultrafast pulsed fiber lasers with good long-term operation stability can be achieved at 1.5 μm and 1 μm, respectively. Our work demonstrates that

C-dots@zeolite could be a new composite material for broadband nonlinear optics and its application in ultrafast photonics.

2. EXPERIMENTAL SECTION

A. Preparation and Characterization of Materials

Zeolite LTA single crystals were hydrothermally synthesized in a reaction system of $1.0Al_2O_3$:$1.0P_2O_5$:2.2NPA:$600H_2O$. Typically, $Al(OiPr)_3$ was added in a solution of H_3PO_4 with distilled water and stirred for 4 h. Then, the NPA was added into the gel solution and stirred for another 2 h. The as-obtained gel was sealed into a teflon-lined stainless-steel autoclave and heated to 190°C for 30 h. The as-synthesized sample was washed with distilled water and dried at 80°C for 3 h. After that, the as-synthesized LTA crystals were placed into a quartz boat and heated from room temperature to 400°C with a heating rate of 5°C/min under vacuum condition. Then, the C-dots@LTA composite was obtained by maintaining 400°C for 3 h. The isolated C-dots were obtained by removing the LTA template. Typically, the as-synthesized C-dots@LTA sample was immersed in hot 3 mol/L NaOH for 2 h and followed by concentrated HCl under ultrasonic treatment. Then, the dark-colored solution was washed with distilled water for six times, and the insoluble samples were centrifugally separated from the solution.

Powder X-ray diffraction (XRD) patterns were collected with a Bruker D8 system. The morphology of the LTA was investigated using a scanning electron microscope (SEM, JEOL Co., Model: JSM-6049LA). The single crystal X-ray diffractometry (Xcalibur, Sapphire3, Gemini Ultra) was carried out for characterizing the structure of crystal. Transmission electron microscopy (TEM) measurements were executed on FEI TECNAI G2 60-300 equipment at an acceleration voltage of 300 kV. The Raman spectrum was obtained using a Horiba JY Labram HR800 with the 514.5 nm laser excitation.

B. Experimental Setup of Fiber Lasers

The laser setup of an erbium-doped fiber laser (EDFL) and ytterbium-doped fiber laser (YDFL) is shown below. A 980 nm laser diode (LD) was used as the pump power source and transmitted into the cavity through a 980/1550 nm wavelength-division multiplexing (WDM) coupler (980/1060 nm for YDFL). An optical isolator (ISO) was placed into the ring laser cavity to ensure the unidirectional propagation of the laser. A polarization controller (PC) was used to adjust the polarization state of light in the cavity. One single LTA zeolite crystal hosting C-dots (C-dots@LTA) was picked onto a fiber optic jumper to form a fiber-compatible SA by using an extra-thin copper wire with the help of an optical microscope and then was inserted into the laser cavity to induce the mode-locked fiber laser operation. The thickness of the C-dots SA is about 100 μm according to the cubic morphology of LTA zeolite. A 10:90 output coupler was used to output the laser. A 1.5-m-long heavily erbium-doped fiber (LIEKKI Er80-8/125, cutoff wavelength: 1250 ± 150 nm, 80 ± 8 dB/m absorption at 1530 nm) with a group velocity dispersion (GVD) of -22.6 ps^2/km at 1550 nm and a 2-m-long heavily ytterbium-doped fiber (LIEKKI Yb1200-4/125, cutoff wavelength: 1010 ± 70 nm, 1200 dB/m absorption at 976 nm) with GVD of 25.6 ps^2/km at 1060 nm were used as the gain medium, respectively. For the EDFL, the other fibers are standard single-mode fiber with a length of 5 m, and the GVD is -17 ps^2/km. As for the YDFL, the other fibers are single-mode fiber (HI 1060) with a length of 4.1 m, and the GVD is 25 ps^2/km. The total laser cavity length is about 6.5 and 6.1 m for EDFL and YDFL, respectively. Thus, the cavity dispersions of EDFL at 1550 nm and YDFL at 1060 nm were estimated at -0.12 ps^2 and 0.15 ps^2, respectively. The output lasers were analyzed by using an optical spectrum analyzer with a resolution of 0.02 nm, a 20 GHz high-speed oscilloscope (Tektronix MSO 72004C) together with a 45 GHz photodetector (New Focus 1014), and a power meter, respectively. The corresponding pulse duration was also measured by an autocorrelator (APE, Pulsecheck SM1200).

3. EXPERIMENTAL RESULTS

Figure 1 illustrates the method to prepare the C-dots@LTA composite with nonlinear saturable absorption properties by *in situ* carbonization of NPA into C-dots in the confined space of zeolite LTA.

First, the LTA crystals were hydrothermally synthesized by using NPA as the structure-directing agent. The powder XRD profile of the as-synthesized sample matches well with the corresponding diffraction results for the simulated XRD pattern of LTA and the other reported XRD pattern of LTA [45,46], indicating phase-pure LTA synthesis with high crystallinity [Fig. 2(a)]. Figure 2(b) shows the corresponding SEM image of zeolite LTA crystals, which have a well-shaped cubic morphology; its average size is about 100 μm. The space group of as-synthesized LTA is *Pm3m* symmetry with lattice constants $a = b = c = 12.02$ Å (1 Å = 0.1 nm), $\alpha = \beta = \gamma = 90°$, and their unit volume is $V = 1736.65$ Å^3, as shown in Fig. 2(c).

Then, the C-dots@LTA composite is obtained by pyrolysis of NPA@LTA at 400°C for 3 h. The TEM characterization of isolated C-dots confirms the narrow size distribution with average size of 2 nm, as shown in Fig. 3(a). The high-resolution TEM image reveals their lattice spacing to be 0.21 nm, which is consistent with the lattice spacing of the (100) plane of graphene [Fig. 3(b)] [47]. The powder XRD pattern of the isolated C-dots shows a broad peak at 26°, corresponding to the characteristic graphitic peak [Fig. 3(c)] [47,48]. The typical D-band (1350 cm^{-1}) and G-band (1590 cm^{-1}) can be clearly observed

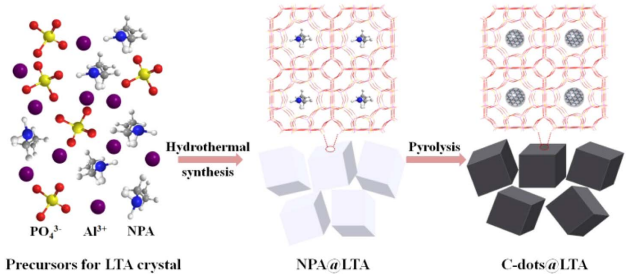

Fig. 1. Schematic of the synthesis process of C-dots@LTA composite material.

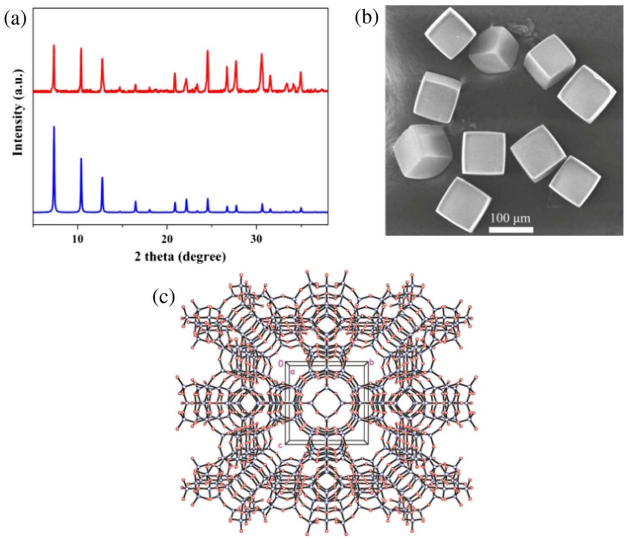

Fig. 2. (a) Experimental (upper) and simulated (lower) XRD patterns of LTA. (b) SEM image of as-synthesized LTA crystals. (c) Framework structure of the LTA single crystal retrieved from single crystal XRD data.

in the Raman spectrum [Fig. 3(d)], agreeing well with other reported C-dots [49,50].

A balanced twin detector measurement system was used to investigate the nonlinear optical characteristics of the as-synthesized C-dots@LTA composite, as shown in Fig. 4(b). The evolution of the absorption ratio was obtained by increasing the pump peak density with home-made pulsed fiber lasers at 1550 nm and 1050 nm, respectively. The data for normalized absorption at 1550 nm and 1050 nm can be well fitted according to a simple two-level saturable model [25,29]. Based on the fitting results, the modulation depth and saturable intensity at 1550 nm are determined to be 7.7% and 7.1 MW·cm^{-2}, respectively [Fig. 4(c)]. Similarly, the modulation depth and saturable intensity at 1050 nm are determined

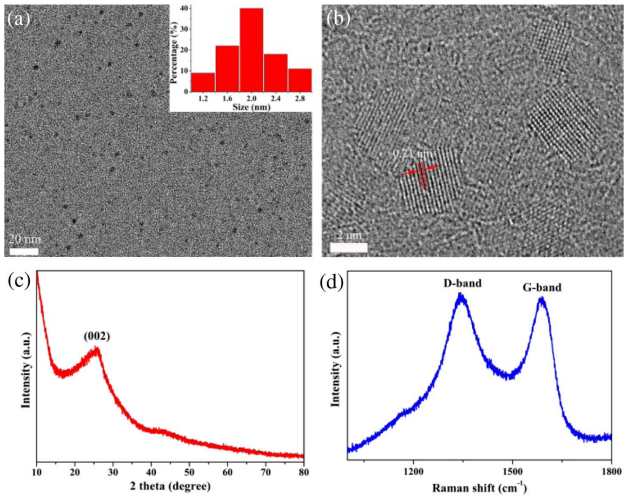

Fig. 3. (a) TEM image (inset: size distribution), (b) high-resolution TEM image, (c) powder XRD pattern, (d) Raman spectrum of as-synthesized C-dots.

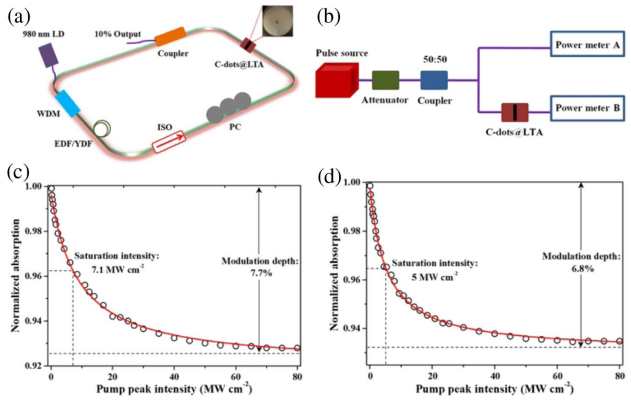

Fig. 4. (a) Schematic diagram of the erbium-doped and ytterbium-doped fiber laser. (b) The setup of a balanced twin-detector measurement. The normalized absorption of the C-dots@LTA SA as a function of pump pulse peak intensity with excitation wavelength of (c) 1550 nm and (d) 1050 nm, respectively: dots, measured data; red line, fitting to the data.

to be 6.8% and 5 MW · cm^{-2}, respectively [Fig. 4(d)]. The modulation depth of the tested C-dots@LTA composite is comparable to other carbon materials [25,29,51], but the normalized nonabsorption loss is larger. This is tolerable for fiber lasers with a relatively large single roundtrip gain coefficient [25,52]. In our case, the contributions to the nonabsorption loss may include scattering and refraction from the surface of LTA zeolite and linear coupling loss between fiber ends. These results clearly demonstrate that the C-dots@LTA composite could be used as an SA for generating ultrafast pulsed lasers in a broad wavelength band.

To explore the applicability of the as-synthesized C-dots@LTA in ultrafast pulsed fiber laser generation, we constructed two all-fiber ring cavities by using EDF and YDF as the gain medium, respectively [Fig. 4(a)]. Before inserting the C-dots@LTA SA into the laser cavity, the laser was insensitive to the polarization state and always worked in the continuous wave mode with an increase in the pump power, which can exclude the nonlinear polarization rotation effect in the laser cavity. As expected, the mode-locking operation of the EDFL was obtained by putting the C-dots@LTA SA into the EDFL cavity when pump power was beyond the mode-locked laser threshold of 150 mW. Figure 5(a) shows the emission spectrum of above mode-locked pulsed fiber laser. The spectrum with two Kelly bands is a typical feature of soliton mode-locked lasers [53]. The operating central wavelength is about 1564.9 nm with a 3 dB spectral bandwidth of 4.84 nm. Figure 5(b) displays a 23 MHz repetition rate of the mode-locked pulse train (period $\tau = 43.5$ ns), which matches well with the laser cavity length (6.5 m). The pulse width is about 609 fs, assuming a sech^2 pulse profile, as shown in Fig. 5(c). Figure 5(d) shows the radio frequency (RF) spectrum of the mode-locked laser output after optical-to-electrical conversion using a fast photodiode. The signal-to-noise ratio (SNR) is over 59 dB, indicating a good mode-locking stability. Figure 5(e) shows the output power of the mode-locked EDFL as a function of the pump power. As the pump power increases from 150 to 310 mW, the output power increases almost linearly from 0.56 to 6.02 mW, resulting

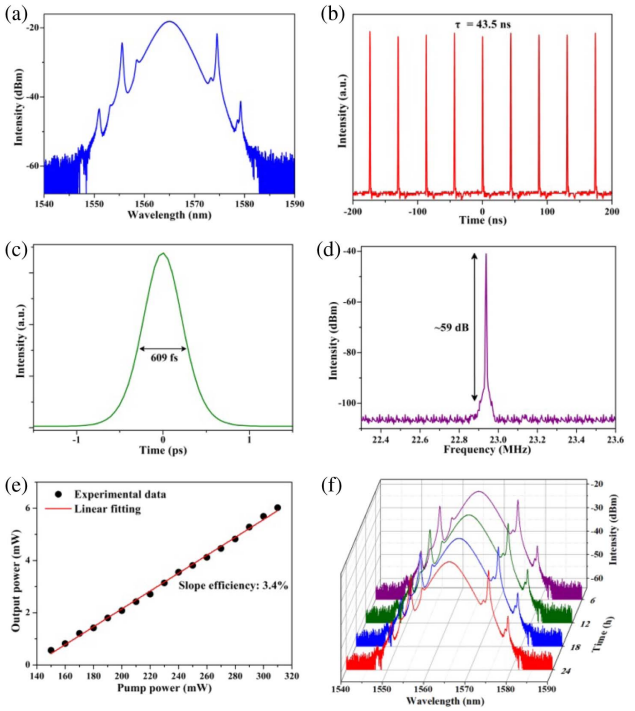

Fig. 5. Output characteristic of the EDFL operated in mode-locking state. (a) Emission spectrum. (b) Pulse train. (c) Single pulse profile. (d) RF spectrum. (e) Output power as a function of the pump power. (f) The output spectrum measured every 6 h showing long-term stability of the mode-locking soliton state.

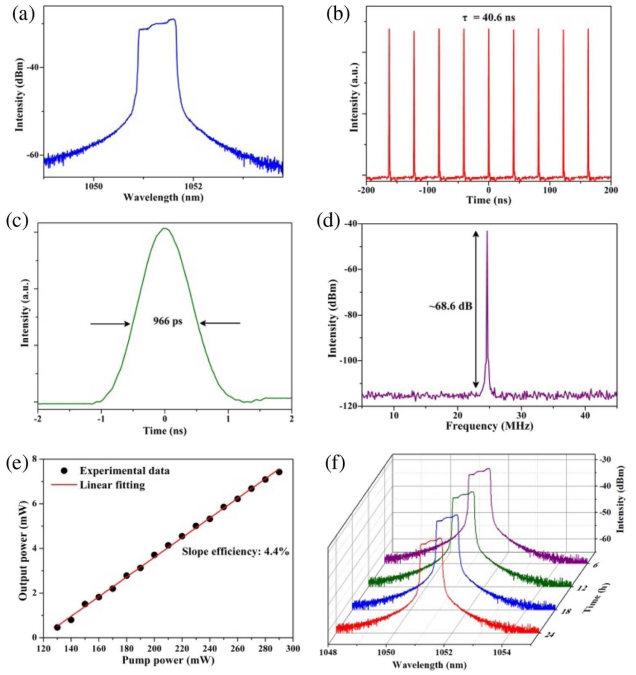

Fig. 6. Output characteristic of the YDFL operated in mode-locking state. (a) Emission spectrum. (b) Pulse train. (c) Single pulse profile. (d) RF spectrum. (e) Output power as a function of the pump power. (f) The output spectrum measured every 6 h showing long-term stability of the mode-locking dissipative soliton state.

in a slope efficiency of 3.4%. Figure 5(f) shows the long-term stability of the mode-locked laser output spectrum measured at 6 h intervals over 1 day. We can clearly find that the mode-locked EDFL is very stable as its central wavelength and the 3 dB bandwidth are kept almost unchanged.

Similarly, the mode-locked YDFL can be obtained by inserting the C-dots@LTA SA into the YDFL cavity when the pump power is beyond the mode-locked laser threshold of 130 mW. The operating central wavelength is about 1051.3 nm with a 3 dB spectral bandwidth of 0.74 nm, as shown in Fig. 6(a). The spectrum with steep edges is a typical shape of dissipative solitons [54]. Figure 6(b) displays a 24.6 MHz repetition rate of the mode-locked pulse train (period $\tau = 40.6$ ns), which matches well with the laser cavity length (6.1 m). The pulse width is about 966 ps, as shown in Fig. 6(c). It is widely known that mode-locked Yb-doped fiber lasers with SAs are mostly dissipative solitons with large chirp, a natural result of the balance among the cavity loss, gain, nonlinearity, and dispersion. Normally, the time bandwidth product (TBP) is widely used to estimate the degree of chirp in pulsed fiber lasers [28,55,56]. The TBP is calculated as 194 in an Yb-doped fiber laser, which means the dissipative solitons are strongly chirped, inducing the expanded pulse duration. The SNR of the RF spectrum is over 68.6 dB, indicating a good mode-locking stability [Fig. 6(d)]. Figure 6(e) shows the output power of the mode-locked YDFL as a function of the pump power. As the pump power increases from 130 to 290 mW, the output power increases almost linearly from 0.46 to 7.42 mW, resulting in a slope efficiency of 4.4%. The mode-locked YDFL is also very stable as its central wavelength and 3 dB bandwidth are kept almost unchanged [Fig. 6(f)]. To estimate the damage threshold of the SA, we increased the pump power to 650 mW (the maximum of the 980 nm LD that we used) and kept it for 2 h. After that, we decreased the pump power from 650 to 0 mW, and both of the stable mode-locked Er-doped and Yb-doped fiber lasers were obtained again in their stable pump power range, which is 150 to 310 mW and 130 to 290 mW, respectively. This means the C-dots@LTA SA is not damaged at the pump power of 650 mW. Thus, the optical damage threshold of the SA is over 650 mW.

Table 1 summarizes data of some reports about mode-locked fiber lasers with a different carbon-based SA. It shows that our C-dots@LTA SA is comparable to other carbon-based SAs, especially for the recently reported novel carbon-based SA [51,57,58]. Moreover, there are some advantages by using C-dots@LTA as the SA to generate ultrafast pulsed fiber lasers. (1) The stability of pulsed fiber lasers is improved, which can be maintained over several months. The LTA zeolite channels offer a solid nanospace to fix C-dots with well dispersion and prevent the aggregation of C-dots. (2) The photonics device is easy to handle. The pulsed fiber lasers can be generated by putting one single LTA zeolite crystal that hosts C-dots between two fiber connectors to form a fiber-compatible SA. (3) The C-dots@LTA SA has a high optical damage threshold, which is over 650 mW. (4) The C-dots@LTA is a cost-effective broadband SA, which can be fabricated at

Table 1. Typical Mode-Locked Fiber Lasers with Different Carbon-Based SAs

SA Type	Wavelength (nm)	Pulse Duration (ps)	SNR (dB)	Slope Efficiency	Reference
Carbon nanotubes	1518–1558	0.706	70		[25]
	1025.5	0.175	63		[28]
Graphene	1565	0.756	65	3%	[29]
	1069.8	580	70		[55]
Graphene oxide	1559.56	0.582	56	2.6%	[57]
Mesoporous carbon	1036	445		2.58%	[51]
Graphdiyne	1564.7	0.734	41.77	1%	[58]
C-dots@LTA	1564.9	0.609	59	3.4%	Our work
	1051.3	966	68.6	4.4%	Our work

a relatively low carbonization temperature of 400°C and can be used for generating Er-doped and Yb-doped pulsed fiber lasers.

4. CONCLUSION

Zeolite LTA single crystals were used as a template for the fabrication of C-dots with a uniform size. The nonlinear optical property of as-synthesized C-dots@LTA composite was investigated, and the application of C-dots@LTA as a new broadband saturable absorber for ultrafast pulsed fiber laser generation was achieved. By inserting the C-dots@LTA SA into the fiber laser cavity, mode-locking operation in EDFL and YDFL with long-term stability was achieved. The mode-locked soliton pulses in EDFL have a central wavelength of 1564.9 nm with the pulse width of 609 fs and repetition rate of 23 MHz. As to the YDFL, the mode-locked dissipative soliton pulses have a central wavelength of 1051.3 nm with a pulse width of 966 ps and repetition rate of 24.6 MHz. Our work reveals the C-dots@zeolite is a promising SA material for ultrafast pulsed fiber laser generation in a broad wavelength band.

Funding. National Key Research and Development Program of China (2016YFA0401100); National Natural Science Foundation of China (61575129, 61705134); Shenzhen Science and Technology Innovation Commission (JCYJ20160328144942069, JCYJ20180305124706833).

REFERENCES

1. X. Xu, R. Ray, Y. Gu, H. J. Ploehn, L. Gearheart, and K. Raker, "Electrophoretic analysis and purification of fluorescent single-walled carbon nanotube fragments," J. Am. Chem. Soc. **126**, 12736–12737 (2004).
2. Y. Xiong, J. Schneider, E. V. Ushakova, and A. L. Rogach, "Influence of molecular fluorophores on the research field of chemically synthesized carbon dots," Nano Today **23**, 124–139 (2018).
3. N. Basu and D. Mandal, "Time-resolved photoluminescence of pH-sensitive carbon dots," Carbon **144**, 500–508 (2019).
4. C. J. Reckmeier, J. Schneider, A. S. Susha, and A. L. Rogach, "Luminescent colloidal carbon dots: optical properties and effects of doping," Opt. Express **24**, A312–A340 (2016).
5. L. Xiao and H. Sun, "Novel properties and applications of carbon nanodots," Nano Scale Horiz. **3**, 565–597 (2018).
6. X. T. Zheng, A. Ananthanarayanan, K. Q. Luo, and P. Chen, "Glowing graphene quantum dots and carbon dots: properties, syntheses, and biological applications," Small **11**, 1620–1636 (2015).
7. I. Milenkovic, M. Algarra, C. Alcoholado, M. Cifuentes, J. M. Lázaro-Martínez, and E. Rodríguez-Castellón, "Fingerprint imaging using N-doped carbon dots," Carbon **144**, 791–797 (2019).
8. X. Gao, C. Du, Z. Zhuang, and W. Chen, "Carbon quantum dot-based nanoprobes for metal ion detection," J. Mater. Chem. C **4**, 6927–6945 (2016).
9. G. A. M. Hutton, B. C. M. Martindale, and E. Reisner, "Carbon dots as photosensitisers for solar-driven catalysis," Chem. Soc. Rev. **46**, 6111–6123 (2017).
10. M. Han, S. Zhu, S. Lu, Y. Song, T. Feng, and S. Tao, "Recent progress on the photocatalysis of carbon dots: classification, mechanism and applications," Nano Today **19**, 201–218 (2018).
11. J. Li, B. Wang, H. Zhang, and J. Yu, "Carbon dots-in-matrix boosting intriguing luminescence properties and applications," Small **15**, 1805504 (2019).
12. B. Kong, J. Tang, Y. Zhang, T. Jiang, X. Gong, and C. Peng, "Incorporation of well-dispersed sub-5-nm graphitic pencil nanodots into ordered mesoporous frameworks," Nat. Chem. **8**, 171–178 (2016).
13. Y. Mu, N. Wang, Z. Sun, J. Wang, J. Li, and J. Yu, "Carbogenic nanodots derived from organo-templated zeolites with modulated full-color luminescence," Chem. Sci. **7**, 3564–3568 (2016).
14. Y. Mu, H. Shi, Y. Wang, H. Ding, and J. Li, "CNDs@zeolite: new room-temperature phosphorescent materials derived by pyrolysis of organo-templated zeolites," J. Mater. Chem. C **5**, 10894–10899 (2017).
15. H. G. Baldovi, S. Valencia, M. Alvaro, A. M. Asiri, and H. Garcia, "Highly fluorescent C-dots obtained by pyrolysis of quaternary ammonium ions trapped in all-silica ITQ-29 zeolite," Nanoscale **7**, 1744–1752 (2015).
16. Y. Wang, Y. Li, Y. Yan, J. Xu, B. Guan, and Q. Wang, "Luminescent carbon dots in a new magnesium aluminophosphate zeolite," Chem. Commun. **49**, 9006–9008 (2013).
17. B. Wang, Y. Mu, H. Yin, Z. Yang, Y. Shi, and J. Li, "Formation and origin of multicenter photoluminescence in zeolite-based carbogenic nanodots," Nanoscale **10**, 10650–10656 (2018).
18. J. Liu, N. Wang, Y. Yu, Y. Yan, H. Zhang, and J. Li, "Carbon dots in zeolites: a new class of thermally activated delayed fluorescence materials with ultralong lifetimes," Sci. Adv. **3**, e1603171 (2017).
19. B. Wang, Y. Mu, H. Zhang, H. Shi, G. Chen, and Y. Yu, "Red room-temperature phosphorescence of CDs@zeolite composites triggered by heteroatoms in zeolite frameworks," ACS Central. Sci. **5**, 349–356 (2019).
20. S. Liu, Q. Wang, K. Wang, Y. Yao, H. Zhang, T. Ren, Z. Yin, F. Du, B. Zhang, and J. He, "Two-photon saturable absorption properties and laser *Q*-switch application of carbon quantum dots," Opt. Lett. **42**, 3972–3975 (2017).
21. F. W. Wise, A. Chong, and W. H. Renninger, "High-energy femtosecond fiber lasers based on pulse propagation at normal dispersion," Laser. Photon. Rev. **2**, 58–73 (2008).
22. K. Ursula, "Recent developments in compact ultrafast lasers," Nature **424**, 831–838 (2003).
23. W. Fu, L. G. Wright, P. Sidorenko, S. Backus, and F. W. Wise, "Several new directions for ultrafast fiber lasers," Opt. Express **26**, 9432–9463 (2018).
24. Z. C. Luo, A. P. Luo, and W. C. Xu, "Tunable and switchable multi-wavelength passively mode-locked fiber laser based on SESAM and inline birefringence comb filter," IEEE Photon. J. **3**, 64–70 (2011).

25. F. Wang, A. G. Rozhin, V. Scardaci, Z. Sun, F. Hennrich, and I. H. White, "Wideband-tuneable, nanotube mode-locked, fibre laser," Nat. Nanotechnol. **3**, 738–742 (2008).
26. J. C. Chiu, C. M. Chang, B. Z. Hsieh, S. C. Lin, C. Y. Yeh, and G. R. Lin, "Pulse shortening mode-locked fiber laser by thickness and concentration product of carbon nanotube based saturable absorber," Opt. Express **19**, 4036–4041 (2011).
27. J. C. Chiu, Y. F. Lan, C. M. Chang, X. Z. Chen, C. Y. Yeh, and C. K. Lee, "Concentration effect of carbon nanotube based saturable absorber on stabilizing and shortening mode-locked pulse," Opt. Express **18**, 3592–3600 (2010).
28. L. Hou, H. Guo, Y. Wang, J. Sun, Q. Lin, and Y. Bai, "Sub-200 femtosecond dispersion-managed soliton ytterbium doped fiber laser based on carbon nanotubes saturable absorber," Opt. Express **26**, 9063–9070 (2018).
29. Q. Bao, H. Zhang, Y. Wang, Z. Ni, Y. Yan, and Z. X. Shen, "Atomic-layer graphene as a saturable absorber for ultrafast pulsed lasers," Adv. Funct. Mater. **19**, 3077–3083 (2009).
30. D. Popa, Z. Sun, F. Torrisi, T. Hasan, F. Wang, and A. C. Ferrari, "Sub 200 fs pulse generation from a graphene mode locked fiber laser," Appl. Phys. Lett. **97**, 203106 (2010).
31. Z. Sun, T. Hasan, F. Torrisi, D. Popa, G. Privitera, and F. Wang, "Graphene mode-locked ultrafast laser," ACS Nano **4**, 803–810 (2010).
32. F. Bonaccorso, Z. Sun, T. Hasan, and A. C. Ferrari, "Graphene photonics and optoelectronics," Nat. Photonics **4**, 611–622 (2010).
33. H. R. Chen, C. Y. Tsai, H. M. Cheng, K. H. Lin, and W. F. Hsieh, "Passive mode locking of ytterbium- and erbium-doped all-fiber lasers using graphene oxide saturable absorbers," Opt. Express **22**, 12880–12889 (2014).
34. J. Boguslawski, J. Sotor, G. Sobon, R. Kozinski, K. Librant, and M. Aksienionek, "Graphene oxide paper as a saturable absorber for Er- and Tm-doped fiber lasers," Photon. Res. **3**, 119–124 (2015).
35. Z. Cheng, H. Li, H. Shi, J. Ren, Q. H. Yang, and P. Wang, "Dissipative soliton resonance and reverse saturable absorption in graphene oxide mode-locked all-normal-dispersion Yb-doped fiber laser," Opt. Express **23**, 7000–7006 (2015).
36. Z. C. Luo, M. Liu, H. Liu, X. W. Zheng, A. P. Luo, and C. J. Zhao, "2 GHz passively harmonic mode-locked fiber laser by a microfiber-based topological insulator saturable absorber," Opt. Lett. **38**, 5212–5215 (2013).
37. Z. Dou, Y. Song, J. Tian, J. Liu, Z. Yu, and X. Fang, "Mode-locked ytterbium-doped fiber laser based on topological insulator: Bi_2Se_3," Opt. Express **22**, 24055–24061 (2014).
38. M. Jung, J. Lee, J. Koo, J. Park, Y. W. Song, and K. Lee, "A femtosecond pulse fiber laser at 1935 nm using a bulk-structured Bi_2Te_3 topological insulator," Opt. Express **22**, 7865–7874 (2014).
39. H. Liu, X. W. Zheng, M. Liu, N. Zhao, A. P. Luo, and Z. C. Luo, "Femtosecond pulse generation from a topological insulator mode-locked fiber laser," Opt. Express **22**, 6868–6873 (2014).
40. K. Yin, B. Zhang, L. Li, T. Jiang, X. Zhou, and J. Hou, "Soliton mode-locked fiber laser based on topological insulator Bi_2Te_3 nanosheets at 2 μm," Photon. Res. **3**, 72–76 (2015).
41. M. Zhang, Q. Wu, F. Zhang, L. Chen, X. Jin, and Y. Hu, "2D black phosphorus saturable absorbers for ultrafast photonics," Adv. Opt. Mater. **7**, 1800224 (2019).
42. W. Liu, L. Pang, H. Han, K. Bi, M. Lei, and Z. Wei, "Tungsten disulphide for ultrashort pulse generation in all-fiber lasers," Nanoscale **9**, 5806–5811 (2017).
43. W. Liu, L. Pang, H. Han, M. Liu, M. Lei, and S. Fang, "Tungsten disulfide saturable absorbers for 67 fs mode-locked erbium-doped fiber lasers," Opt. Express **25**, 2950–2959 (2017).
44. R. Lü, Y. Wang, J. Wang, W. Ren, L. Li, and S. Liu, "Soliton and bound-state soliton mode-locked fiber laser based on a MoS_2/fluorine mica Langmuir-Blodgett film saturable absorber," Photon. Res. **7**, 431–436 (2019).
45. X. Guo and A. Navrotsky, "Hydration dynamics in zeolite A—an X-ray diffraction and infrared spectroscopic study," Micropor. Mesopor. Mater. **268**, 197–201 (2018).
46. C. Chen, D. Zhai, L. Dong, Y. Wang, J. Zhang, and Y. Liu, "Organic anions facilitate *in situ* synthesis of mesoporous LTA zeolites," Chem. Mater. **31**, 1528–1536 (2019).
47. S. N. Baker and G. A. Baker, "Luminescent carbon nanodots: emergent nanolights," Angew. Chem. Int. Ed. **49**, 6726–6744 (2010).
48. D. Pan, J. Zhang, Z. Li, and M. Wu, "Hydrothermal route for cutting graphene sheets into blue-luminescent graphene quantum dots," Adv. Mater. **22**, 734–738 (2010).
49. S. Zhang, L. Sui, H. Dong, W. He, L. Dong, and L. Yu, "High-performance supercapacitor of graphene quantum dots with uniform sizes," ACS Appl. Mater. Interface **10**, 12983–12991 (2018).
50. X. Meng, Q. Chang, C. Xue, J. Yang, and S. Hu, "Full-colour carbon dots: from energy-efficient synthesis to concentration-dependent photoluminescence properties," Chem. Commun. **53**, 3074–3077 (2017).
51. F. Wang, Y. Jing, Z. Kang, L. Zhou, Z. Li, and M. Liu, "Mesoporous carbon nanospheres as broadband saturable absorbers for pulsed laser generation," Adv. Opt. Mater. **6**, 1800606 (2018).
52. K. H. Fong, S. Y. Set, R. Grange, A. Schlatter, K. Kikuchi, and C. S. Goh, "Solid-state Er:Yb:glass laser mode-locked by using single-wall carbon nanotube thin film," Opt. Lett. **32**, 38–40 (2007).
53. F. X. Kartner, I. D. Jung, and U. Keller, "Soliton mode-locking with saturable absorbers," IEEE J. Sel. Top. Quantum Electron. **2**, 540–556 (1996).
54. P. Grelu and N. Akhmediev, "Dissipative solitons for mode-locked lasers," Nat. Photonics **6**, 84–92 (2012).
55. L. M. Zhao, D. Y. Tang, H. Zhang, X. Wu, Q. Bao, and K. P. Loh, "Dissipative soliton operation of an ytterbium-doped fiber laser mode locked with atomic multilayer graphene," Appl. Phys. Lett. **35**, 3622–3624 (2010).
56. P. Li, Y. Chen, T. Yang, Z. Wang, H. Lin, and Y. Xu, "Two dimensional $CH_3NH_3PbI_3$ perovskite nanosheets for ultrafast pulsed fiber lasers," ACS Appl. Mater. Interfaces **9**, 12759–12765 (2017).
57. Z. Chen, H. Wang, Y. Wang, R. Lv, X. Yang, and J. Wang, "Improved optical damage threshold graphene oxide/SiO_2 absorber fabricated by sol-gel technique for mode-locked erbium-doped fiber lasers," Carbon **144**, 737–744 (2019).
58. Y. Zhao, P. Guo, X. Li, and Z. Jin, "Ultrafast photonics application of graphdiyne in the optical communication region," Carbon **149**, 336–341 (2019).